Research Article

Jiale Zhao, Bing Zhou*, Guanglong Wang, Jie Liu*, Jiaju Ying, Qi Chen, and Runze Zhao

# Spectral uncertainty analysis of grassland and its camouflage materials based on land-based hyperspectral images

https://doi.org/10.1515/phys-2023-0157
received July 05, 2023; accepted November 14, 2023

**Abstract:** Spectral uncertainty is one of the most prominent spectral characteristics of hyperspectral images. Compared to the process of remote sensing hyperspectral imaging, hyperspectral imaging under land-based imaging conditions has the characteristics of variable detection directions, random imaging times, and complex environmental conditions, resulting in increased spectral uncertainty of targets in land-based hyperspectral images. The spectral uncertainty of the target mainly refers to the phenomenon of "Same spectral reflectance but different objects" and "Same object but different spectral reflectance" which poses significant difficulties for subsequent hyperspectral image target detection and recognition. In order to analyze the spectral uncertainty of hyperspectral images in land-based applications and address the issue of spectral uncertainty in similar targets, a spectral uncertainty evaluation index based on standard deviation vector was proposed. For the overall spectral separability between different types of targets, a quantitative index based on Jaccard Distance (JD-SSI) is proposed to measure the spectral separability of different kinds of targets. The experiment focused on grassland and its four typical camouflage materials, analyzing the spectral intra class differences and inter class separability of each target with grassland. It is a fundamental work for studying the spectral characteristics of land-based hyperspectral images, providing a new approach for subsequent spectral band extraction, hyperspectral image classification, and target detection tasks.

**Keywords:** hyperspectral imaging, spectral uncertainty, camouflage materials, Jaccard distance, spectral separability

## 1 Introduction

The emergence of hyperspectral imaging technology fully combines the spectrum of ground objects determined by material composition with the spatial form reflecting the structure of ground objects, that is, endowing each pixel containing ground object targets with specific spectral information [1–3]. The hyperspectral imaging technology appeared in the early 1980s, and has received widespread attention from scholars at home and abroad in the past few decades [4–6]. It has been widely used in mineral research [7], agriculture [8–11], environmental detection [12], and other fields [13–16]. In recent years, with the rapid development of ground unmanned platforms and drone technology, research on the characteristics and applications of land-based hyperspectral images has emerged endlessly [17–20]. There are significant differences between hyperspectral remote sensing imaging and land-based hyperspectral imaging in terms of imaging conditions, imaging processes, analysis methods, *etc.* This also leads to different characteristics and processing methods between land-based hyperspectral images and hyperspectral remote sensing images.

The factors that lead to the uncertainty of the target spectrum can be mainly attributed to three aspects: the properties and structure of the ground object itself, the environmental conditions during the imaging process, and the imaging parameters such as detection direction [21,22]. Land-based hyperspectral images have high spatial resolution and can distinguish more detailed structural information of objects which increases the spectral uncertainty of the target. In practical applications, the properties, morphology,

* **Corresponding author: Bing Zhou,** Department of Electronic and Optical Engineering, PLA Army Engineering University, Shijiazhuang 050000, China, e-mail: bzhou2022@163.com
* **Corresponding author: Jie Liu,** Department of Electronic and Optical Engineering, PLA Army Engineering University, Shijiazhuang 050000, China, e-mail: yclj07@163.com
**Jiale Zhao, Jiaju Ying, Qi Chen:** Department of Electronic and Optical Engineering, PLA Army Engineering University, Shijiazhuang 050000, China
**Guanglong Wang:** Department of Missile Engineering, PLA Army Engineering University, Shijiazhuang 050000, China
**Runze Zhao:** Department of Equipment Command and Management, PLA Army Engineering University, Shijiazhuang 050000, China

and environmental conditions of the target are relatively fixed. Therefore, imaging parameters such as detection direction conditions have a significant impact on the spectral characteristics of the target [23,24]. Remote sensing imaging generally adopts a vertical detection method, and the detection time is relatively fixed. However, the detection direction is random and the imaging time is not fixed under land-based imaging conditions. Therefore, the spectral uncertainty of land-based hyperspectral images is enhanced.

The common methods for evaluating spectral similarity include spectral angle mapping (SAM) [25], similarity evaluation based on Euclidean distance [26], and similarity evaluation based on correlation coefficient (CC) [27]. When studying the spectral similarity between objects, the above methods generally choose the average value of the target spectral curve to represent the spectral value of the target, ignoring the intra class differences of the target [28–30]. As the spectral uncertainty factors of targets in land-based hyperspectral images increase, it is necessary to fully consider the spectral uncertainty issues when measuring the similarity between two objects. This study focuses on grassland and its camouflages, quantifying the spectral uncertainty of targets and the spectral separability between two targets which has significant practical significance.

# 2 Methods

## 2.1 Jaccard distance

Jaccard distance is an indicator used to measure the difference between two sets, which is a complement to the Jaccard similarity coefficient [31]. The Jaccard similarity coefficient, also known as the Jaccard Index, is an indicator used to measure the similarity between two sets. Jaccard similarity coefficient is mainly applied in paper duplication checking systems, exam cheating prevention systems, and other aspects [32,33].

The Jaccard coefficient is mainly used to calculate the similarity between samples. The calculation method for Jaccard similarity coefficient is: the ratio of sample intersection to sample union, represented by $J(A, B)$, as shown in formula (1).

$$J(A, B) = \frac{|A \cap B|}{|A \cup B|}. \tag{1}$$

Similarly, Jaccard Distance is represented by $d_J(A, B)$, as shown in formula (2).

$$d_J(A, B) = 1 - J(A, B) = 1 - \frac{|A \cap B|}{|A \cup B|}. \tag{2}$$

## 2.2 Degree of spectral uncertainty of objects and spectral separability index between different objects of the same class

The spectral reflectance characteristics exhibited by objects under different conditions are different, and the values of spectral reflectance have a certain range of variation at specific wavelengths. Assuming that the spectral range of the imaging system is divided into N bands, and the reflectivity at $\lambda_i$ ($I = 1...N$) is $R_i$, which varies within the range of $[R_{i\min}, R_{i\max}]$ due to various uncertain factors. As shown in Figure 1, $R_{i\min}$ represents the minimum value of reflectivity under various changing conditions at point $\lambda_i$, $R_{i\max}$ represents the maximum value of reflectivity under the influence of various changing conditions at point $\lambda_i$, and $R_{i\text{aver}}$ represents the average reflectance under the influence of various changing conditions at point $\lambda_i$.

The spectral uncertainty of objects of the same category can be represented by the spectral standard deviation vector. The standard deviation of reflectivity at point $\lambda_i$ represents the degree of spectral uncertainty at point $\lambda_i$. Assuming the number of samples to be tested is $K$, the $K$-th sample is $\lambda$. If the reflectivity is $R_{ik}$, then the spectral uncertainty of the object can be determined by $S(\lambda_i)$, as shown in formula (3).

$$S(\lambda_i) = \frac{\sum_{k=1}^{K} (R_{ik} - R_{i\text{aver}})^2}{K}. \tag{3}$$

Considering the spectral uncertainty of objects, in order to measure the spectral separability between different types of objects, a quantitative indicator of spectral

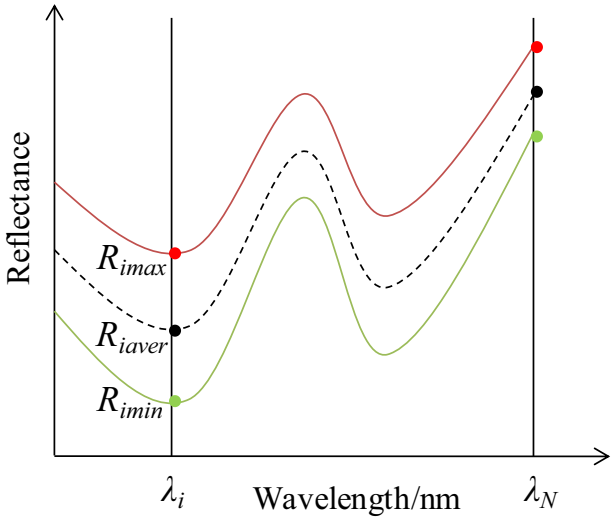


**Figure 1:** Schematic diagram of the variation range of object spectral reflectance.

separability based on the Jaccard Distance is proposed. $R_{ik}^{A}$ represents the reflectance in the $K$-th sample of Class A at point $\lambda_i$, $R_{max}^{A}$ represents the maximum value of reflectance of all samples of Class A at point $\lambda_i$ and $R_{min}^{A}$ represents the minimum spectral reflectance of all samples of Class A. Similarly, a physical quantity superscripted with B represents the reflectance of Class B. As shown in Figure 2, the spectral curves of two types of objects (A and B) can be mainly divided into three situations. Combined with the definition of Jaccard distance, $M(\lambda_i)$ can be used to represent the spectral separability at $\lambda_i$ between A and B, as shown in formula (4), where Eqs. ② and ③ represent the intersection of spectral ranges.

$$M(\lambda_i) = \begin{cases} 1, [R_{i\min}^{A}, R_{i\max}^{A}] \cap [R_{i\min}^{B}, R_{i\max}^{B}] = \varnothing \quad (1) \\ 1 - \dfrac{R_{i\max}^{B} - R_{i\min}^{A}}{R_{i\max}^{A} - R_{i\min}^{B}}, R_{i\max}^{A} \geq R_{i\max}^{B} \geq R_{i\min}^{A} \\ \qquad\qquad \geq R_{i\min}^{B} \quad (2) \\ 1 - \dfrac{R_{i\max}^{A} - R_{i\min}^{B}}{R_{i\max}^{B} - R_{i\min}^{A}}, R_{i\max}^{B} \geq R_{i\max}^{A} \geq R_{i\min}^{B} \\ \qquad\qquad \geq R_{i\min}^{A} \quad (3) \\ 0, [R_{i\min}^{A}, R_{i\max}^{A}] \\ \qquad\qquad \subset [R_{i\min}^{B}, R_{i\max}^{B}] \\ \qquad\qquad \text{or}[R_{i\min}^{A}, R_{i\max}^{A}] \\ \qquad\qquad \supset [R_{i\min}^{B}, R_{i\max}^{B}] \quad (4). \end{cases} \tag{4}$$

When the situation shown in box a occurs, A and B are completely unclassifiable. In the case shown in box b, A and B are completely classifiable. If the range of changes in the spectral curves of two objects is as shown in box c, $M(\lambda_i)$ can be used to measure their specific separability.

# 3 Experiments

## 3.1 Experimental design and data acquisition

The ideal scenario for studying the spectral uncertainty of an object is to have a spectral reflectance database of the target object under any conditions that meet the application requirements. However, it is impossible to measure the spectral reflectance of the target in all cases for research in practical applications. Sampling and statistical methods are often used to obtain information. In the experiment, an imaging spectrometer was used to capture hyperspectral images. In order to obtain more representative sample spectral reflectance, it is planned to conduct multiple experiments at different detection orientations, scene conditions, and target shapes to obtain the spectral reflectance of the target. As shown in Figure 3, set the target position at the center and keep the light source (referred to as the sun) at 0° azimuth angle. The red dot represents the detection angle information selected for the experiment, and its polar coordinate value represents the relative azimuth angle between the light source and the detector. The vertical axis coordinate value represents the detection altitude angle.

Using a field imaging spectrometer to measure the directional spectral reflectance of ground objects, a band interval of 4 nm was set, and 89 band images were obtained within the spectral range of 449–801 nm. Each image recorded the radiance values of the ground objects at different wavelengths. Polytetrafluoroethylene (PTFE) is used as a standard whiteboard, and the directional reflection characteristics of PTFE materials are relatively uniform and can be

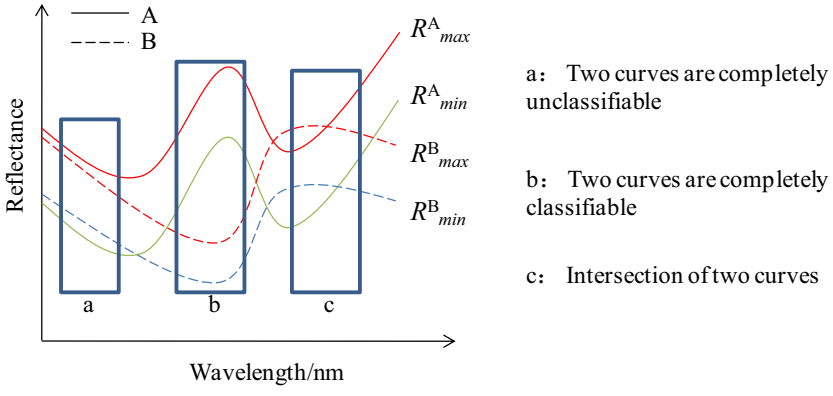


**Figure 2:** Three different situations of the spectral reflectivity range of two types of objects.

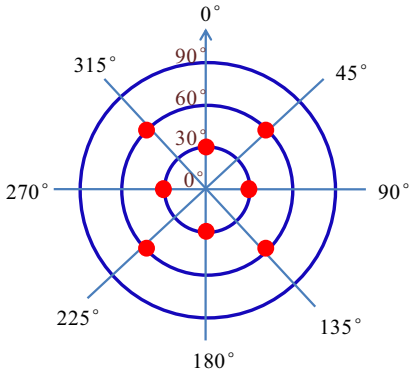


**Figure 3:** Schematic diagram of measurement conditions.

approximated as Lambertian bodies in the range of 400–2,500 nm. The measured features include four common types of grassland camouflage clothing, represented by A, B, C, and D, as shown in Figure 4.

## 3.2 Spectral reflectance of grassland and its four camouflage materials

Experiments were completed using an imaging spectrometer under eight different conditions, and eight sets of land-based hyperspectral images were obtained. The pixel area containing the target was sampled, and 100 spectral reflectance curves of various tested targets were obtained from each set of data for further research. The spectral reflectance was measured using formula (5) [34].

$$R(\lambda) = \frac{L_o(\lambda)}{L_p(\lambda)} \times \rho. \tag{5}$$

where $R(\lambda)$ represents the spectral reflectance of an object, $L_o(\lambda)$ represents the radiance value of an object, and $L_p(\lambda)$ represents the radiance value of the standard plate, $\rho$ represents the reflectivity of the standard plate, which is generally a constant, taken as 0.98. The measured grassland and camouflage materials A, B, C, and D under different conditions are shown in Figures 5–9.

Based on the above experimental results, extracting the extreme values of spectral reflectance under all conditions can obtain the range of spectral reflectance changes for this type of object. The spectral reflectance variation range of the grassland is shown in Figure 10, and the spectral reflectance variation range of camouflage A, B, C, and D is shown in Figure 11. The red line represents the upper limit of reflectivity, while the black line represents the lower limit of reflectivity.

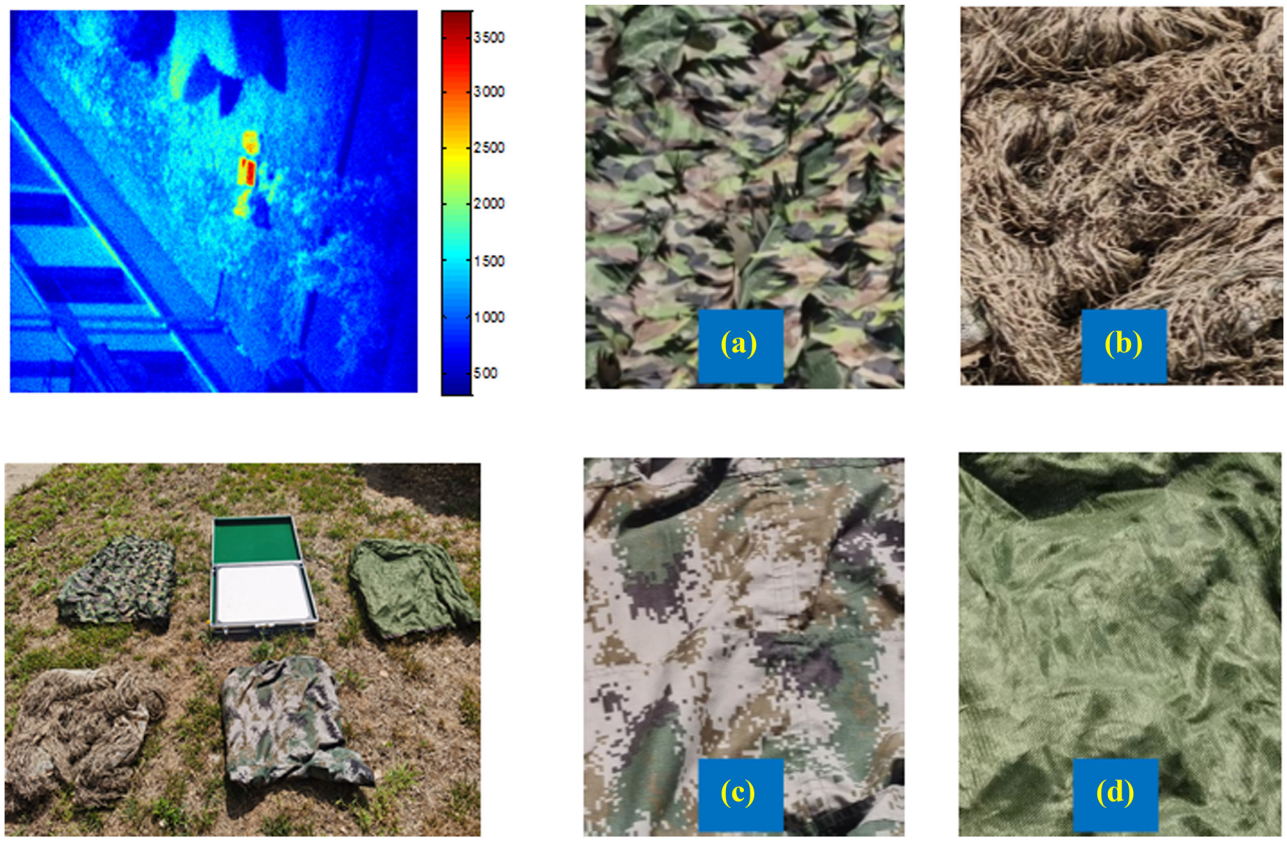


**Figure 4:** The experimental area and four different camouflage materials A, B, C, and D.

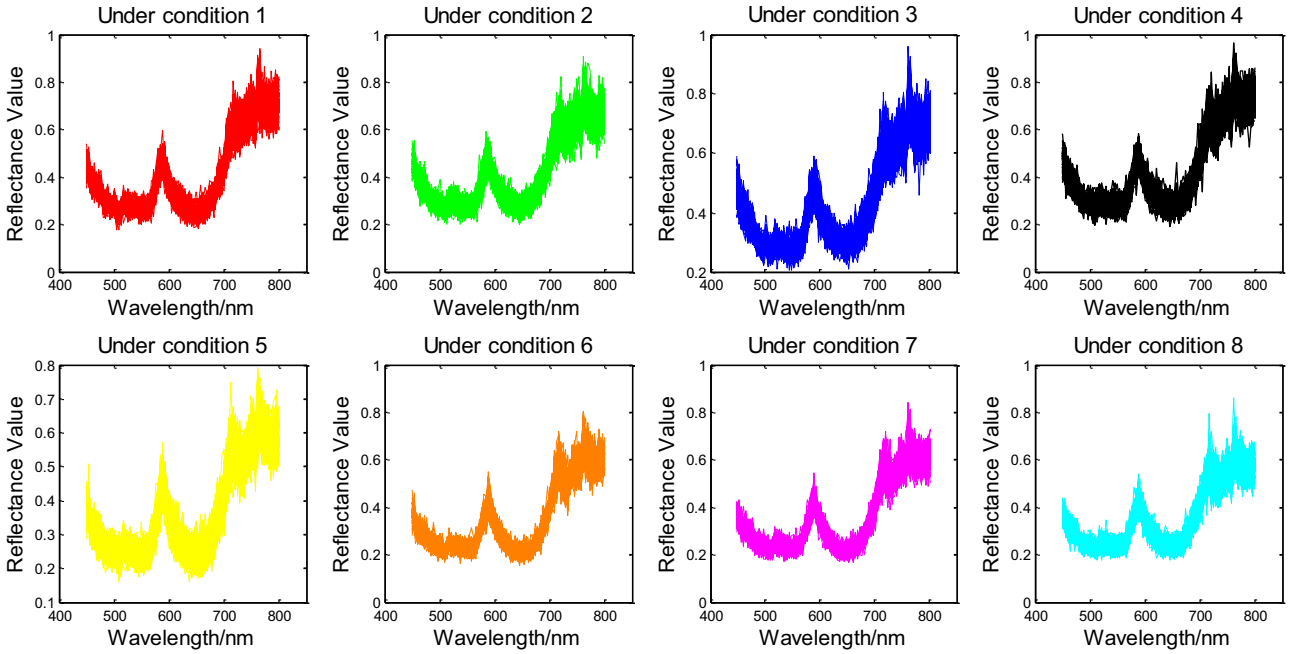


**Figure 5:** Spectral reflectance of grassland under eight experimental conditions.

## 3.3 Quantitative analysis of spectral uncertainty of grassland and its four types of camouflage objects

After the above analysis, the spectral reflectance range of each object can be obtained. In order to study the intra-class uncertainty of the object, the standard deviation vector is used to measure the degree of dispersion of spectral reflectance changes. By substituting the reflectance of the object to be measured in formula (3), the standard deviation vectors of various target spectral reflectance can be obtained, as shown in Figure 12.

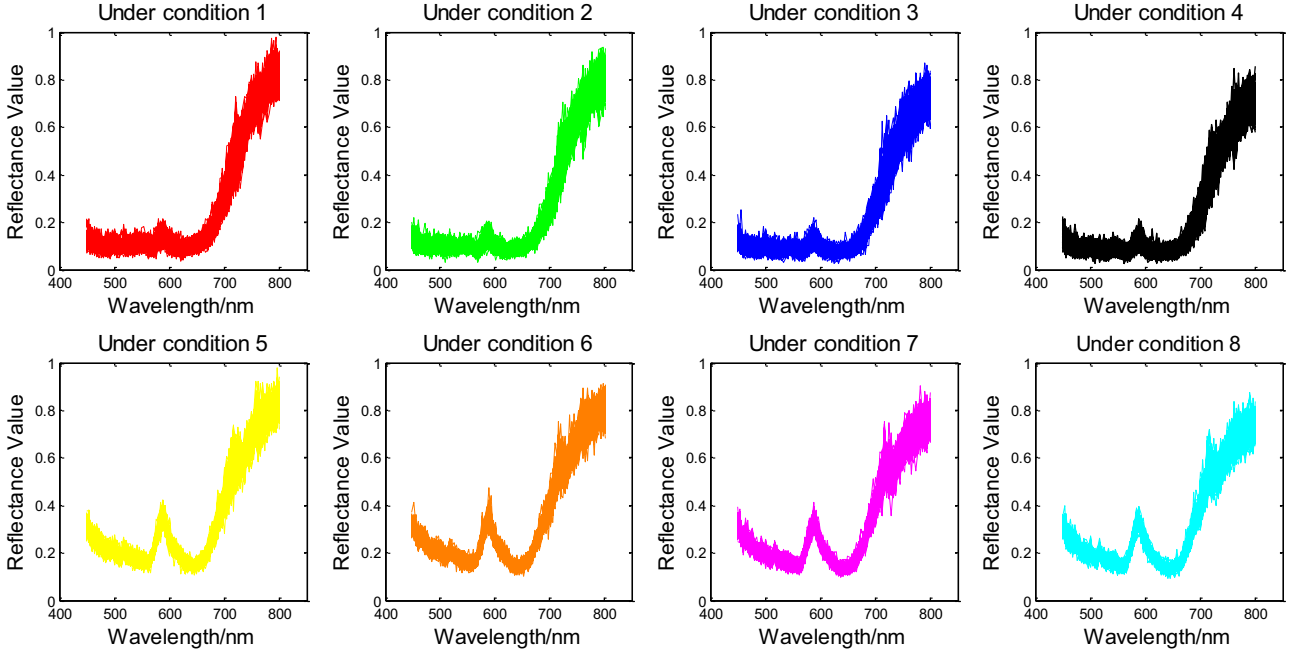


**Figure 6:** Spectral reflectance of A under eight experimental conditions.

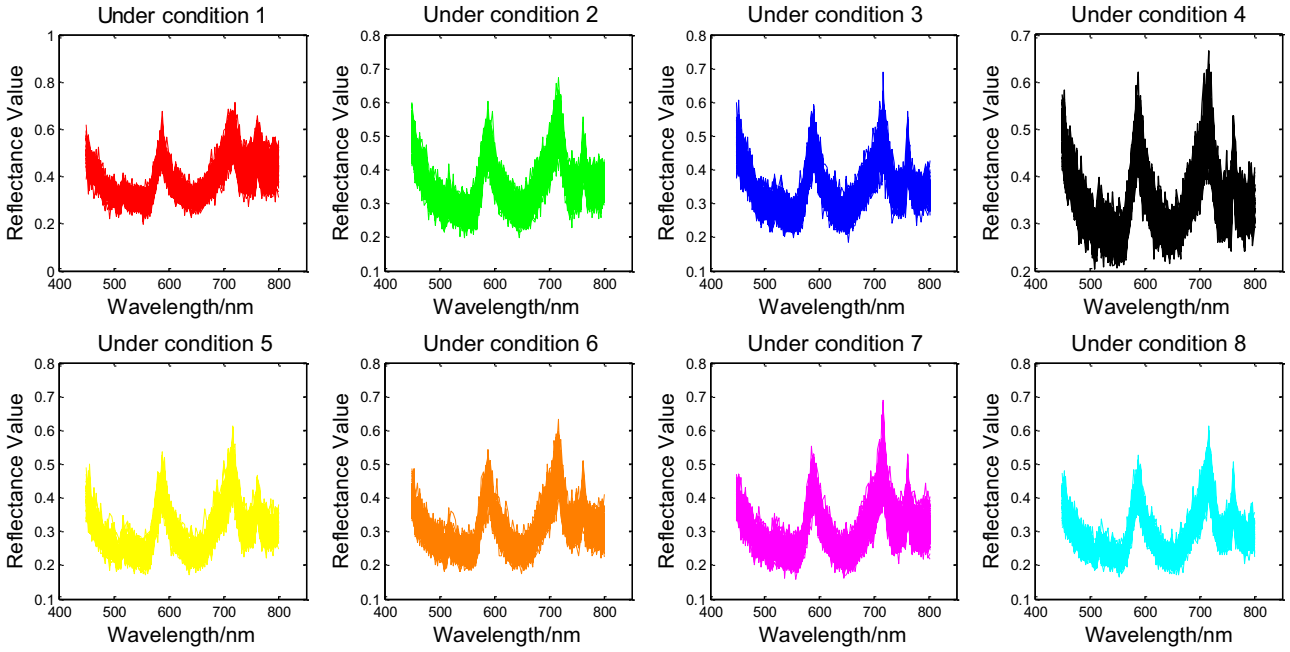


**Figure 7:** Spectral reflectance of B under eight experimental conditions.

From Figure 12, it can be seen that the standard deviation vectors of several objects have similar changing trends. Among them, the standard deviation vectors of the spectral reflectance of object B and grassland are the most similar, while the standard deviation vectors of A, C, and D are relatively close, but there are significant differences between them and grassland. All the standard deviation vectors of the five targets have minimum values near 550, 650, and 750 nm, indicating that the spectral reflectance of grassland and its camouflages fluctuates less and is relatively stable near these three wavelengths.

In order to study the spectral separability between different types of targets, the method proposed by formula (4) was used to calculate the spectral separability

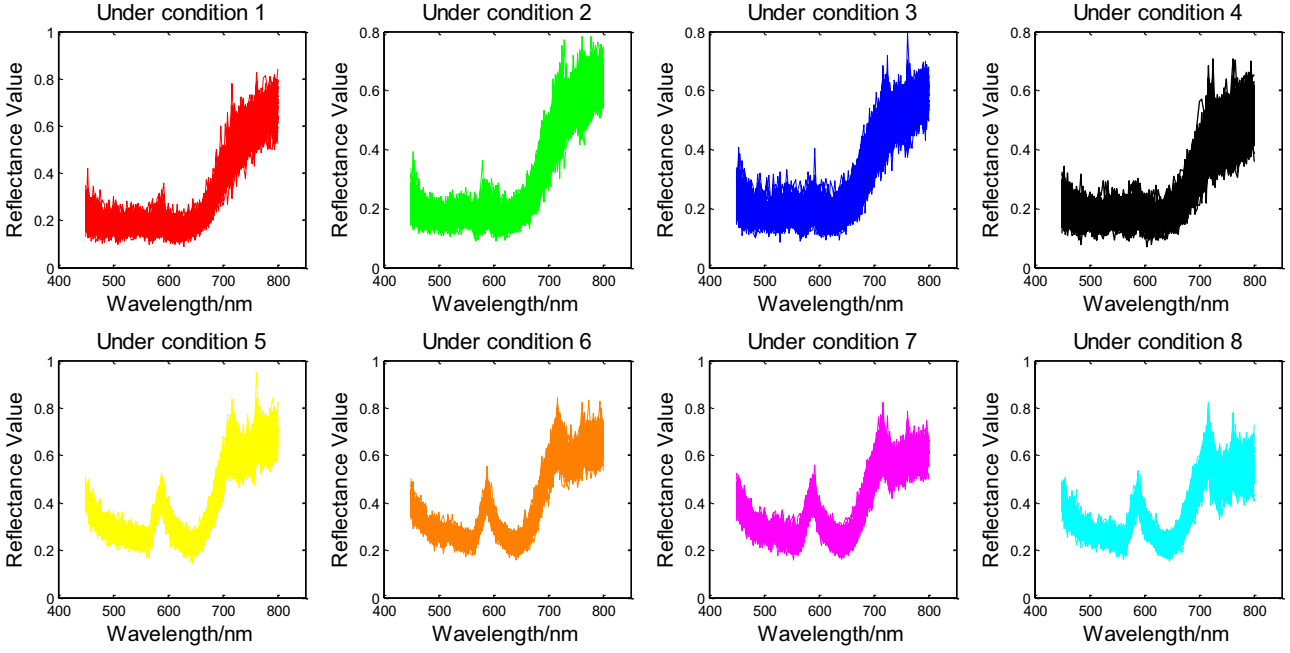


**Figure 8:** Spectral reflectance of C under eight experimental conditions.

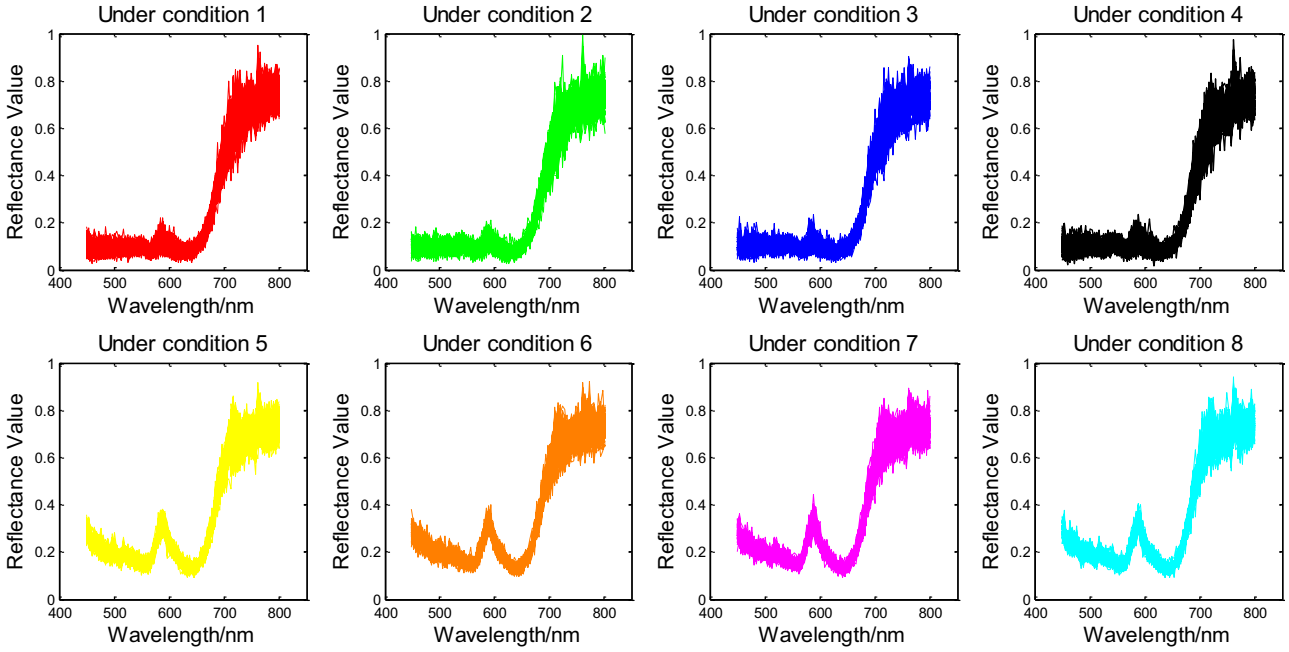


**Figure 9:** Spectral reflectance of D under eight experimental conditions.

indicators of grassland and four types of camouflage objects A, B, C, and D. The results are shown in Figures 13–16. The larger the spectral separability index, the greater the spectral difference between the two objects in the corresponding band. The smaller the spectral separability index, the greater the spectral similarity and difficulty in distinguishing between the two objects in the corresponding band.

From the perspective of spectral uncertainty, it can be found that the spectrum of object A differs significantly from that of grassland before 650 nm, but the spectral similarity increases after 650 nm. The spectral reflectance of object B and grassland is generally similar, but there is a significant difference after 700 nm. The C object does not have a completely distinguishable band from the grassland, and the spectral distinguishability remains at a low level, which has a good effect in practical camouflage applications. Objects D and A have similar characteristics, the spectral similarity between object D and grassland is relatively high after 650 nm.

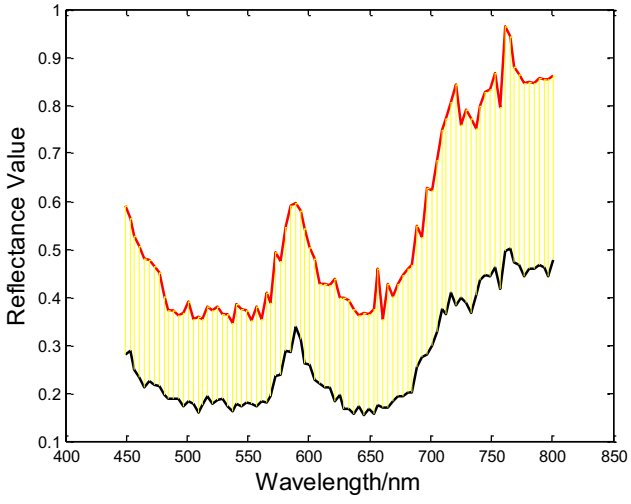


**Figure 10:** Spectral reflectance variation range of grassland.

## 3.4 Study on spectral similarity between grassland and four typical camouflage objects

This article uses SAM, standard deviation method (StDev), and spectral correlation coefficient method (SCC) as comparative methods [35]. The formulas for the three methods are given in in formulas (6)–(8) The two spectral reflection vectors are $X$ and $Y$.

$$\theta = \arccos \frac{\sum_{i=1}^{n} x_i \cdot y_i}{\sqrt{\sum_{i=1}^{n} x_i^2} \cdot \sqrt{\sum_{i=1}^{n} y_i^2}}, \tag{6}$$

where $\theta$ is the generalized included angle of two variables. The smaller the value of $\theta$ is, the higher the similarity of spectral curve shape is, and better the camouflage effect is. n represents the spectral dimension.

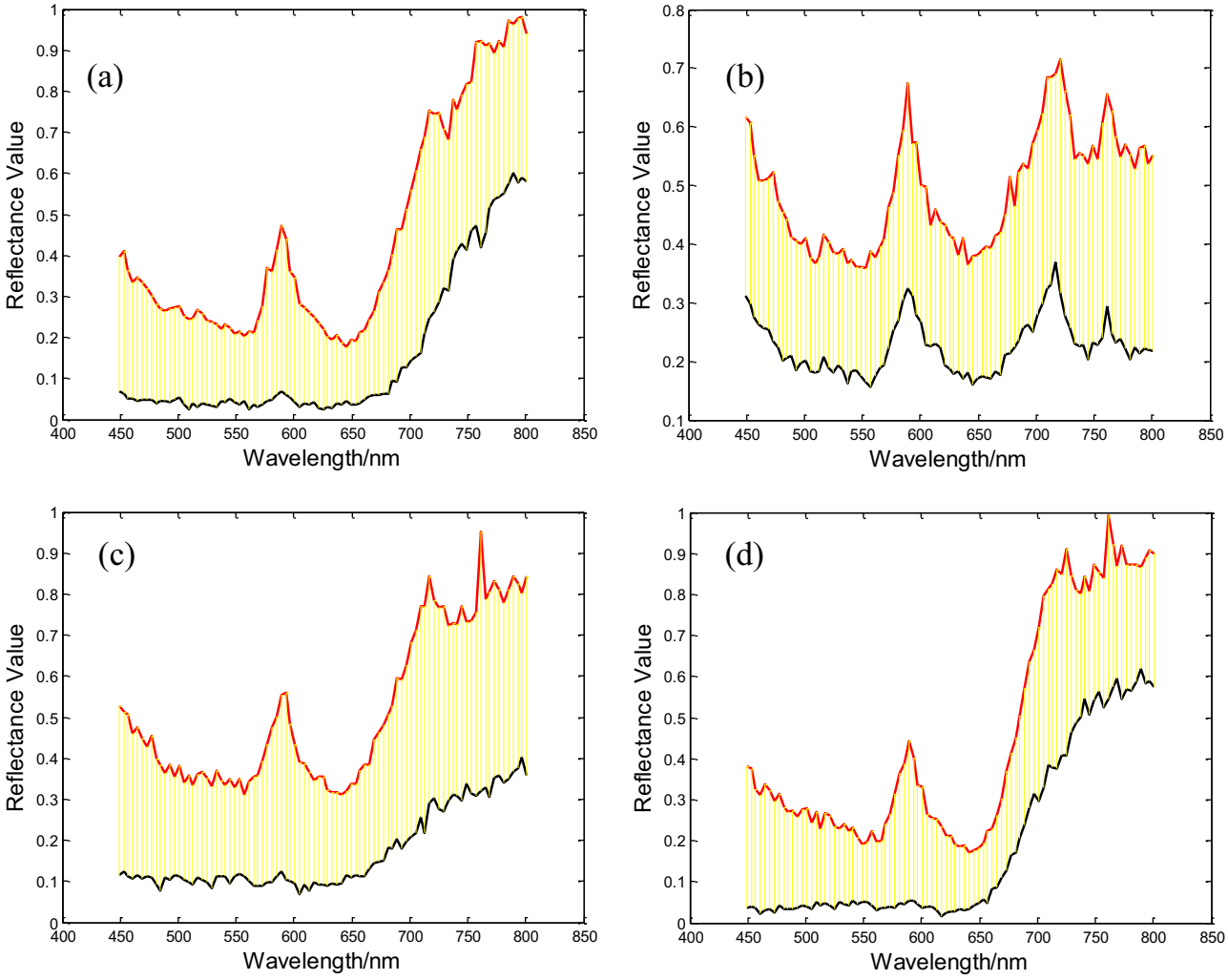


**Figure 11:** Spectral reflectance variation range of four types of camouflage materials A, B, C, and D.

$$S = \sqrt{\frac{1}{n-1}\sum_{i=1}^{n}(x_i - y_i)^2}, \tag{7}$$

where $S$ is the generalized included angle of two variables. The smaller the value of $S$ is, the higher the numerical similarity of the spectral curve is, and the better the camouflage effect is. n represents the spectral dimension.

$$r = \frac{\sum_{i=1}^{n}(x_i - \overline{x})(y_i - \overline{y})}{\sqrt{\sum_{i=1}^{n}(x_i - \overline{x})^2 \times (y_i - \overline{y})^2}}. \tag{8}$$

The CC of two variables $X$ and $Y$ is often expressed by $r$. The greater the correlation $r$, the stronger the correlation.

Calculating the spectral similarity between two objects requires the use of two representative spectral curves. Usually, the average reflectance of the target spectrum within a uniform area is chosen to represent the target spectrum. Land-based hyperspectral images enhance the

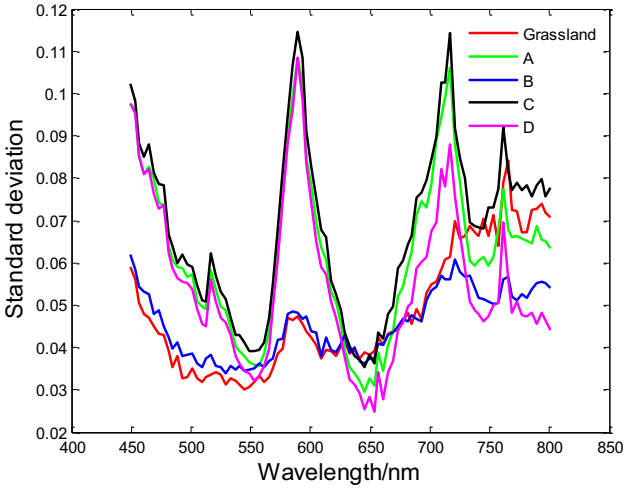


**Figure 12:** Standard deviation vectors of spectral reflectance for various targets.

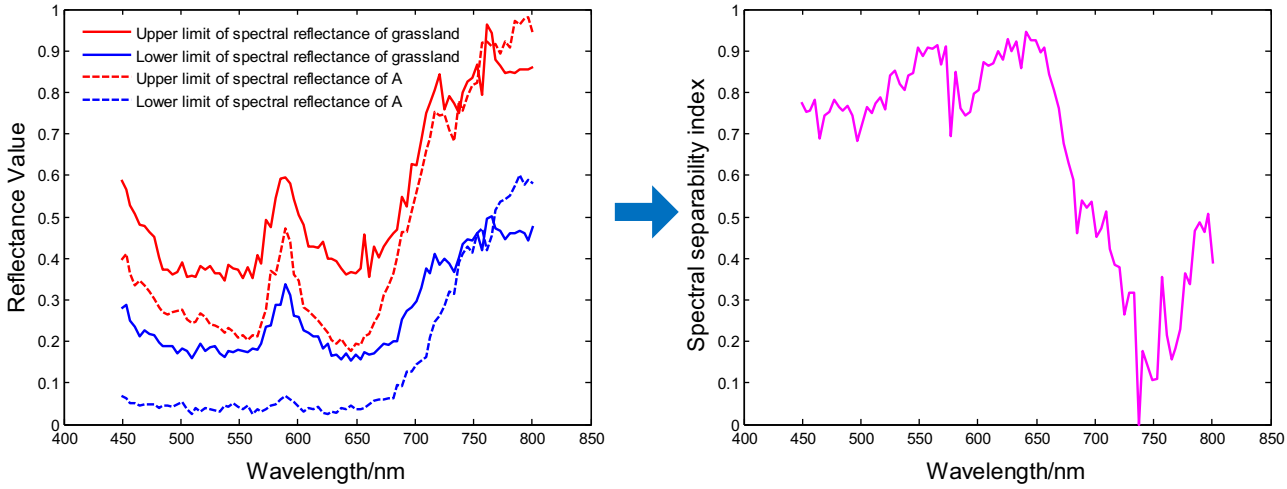


**Figure 13:** JD-SSI values between grassland and A.

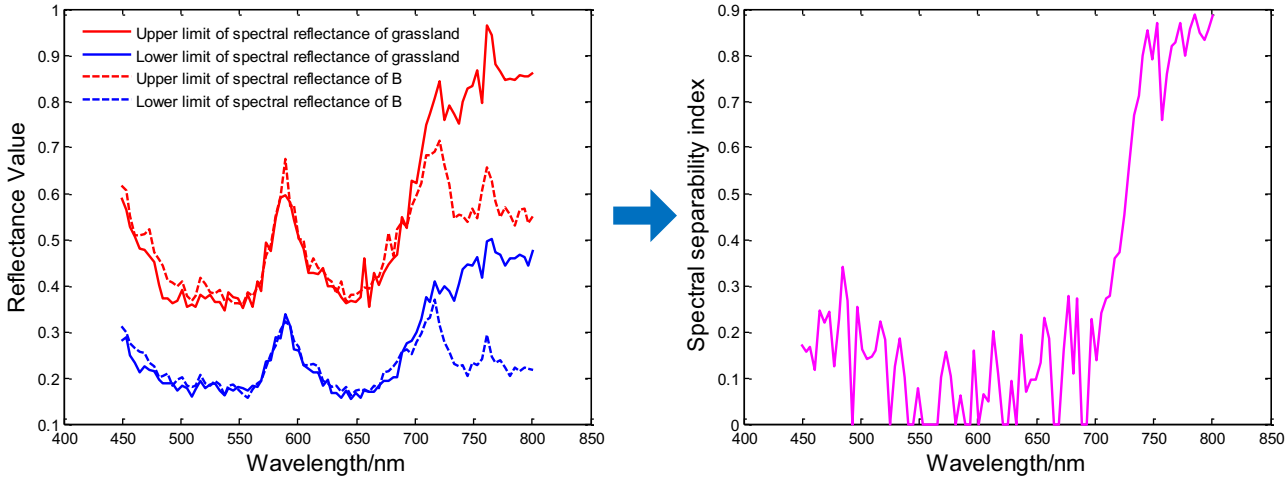


**Figure 14:** JD-SSI values between grassland and B.

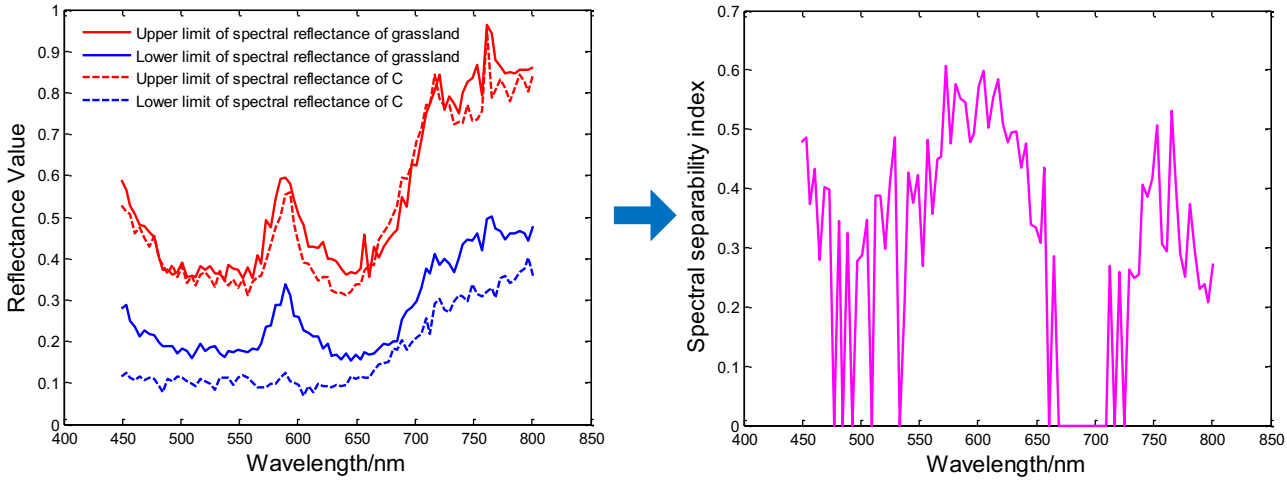


**Figure 15:** JD-SSI values between grassland and C.

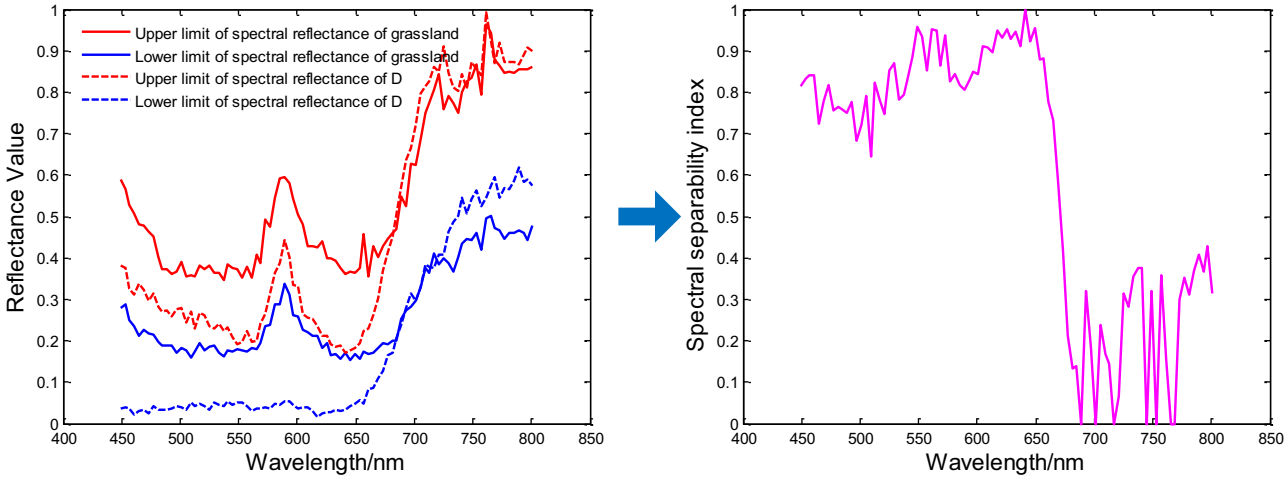


**Figure 16:** JDSSI values between grassland and D.

uncertainty of the target spectrum to a certain extent, which makes traditional spectral similarity calculation methods problematic. The purpose of spectral band selection is to remove redundant bands and screen out the most discriminative bands. In other words, selecting a certain number of spectral bands reduces the intra-class distance and increases the inter-class distance of the spectrum. According to the above analysis, the spectral standard deviations of grasslands and their camouflages have minimal values at 550, 650, and 750 nm, resulting in small intra class distances. Therefore, the focus is on analyzing these wavelength ranges. The spectral similarity between the grassland and various camouflages is shown in Table 1.

SAM, StDev, and JD-SSI all have higher values indicating greater spectral separability and lower spectral similarity. The larger the numerical value of SCC, the higher the spectral similarity and the poorer the spectral separability. In Table 1, the similarity extremum values for different types of camouflage in the four similarity evaluation methods in the range of 449–801 nm were marked in bold and the bands with the most separability for each method were also marked.

Overall, the spectral similarity between grassland and objects A and B is poor, while the spectral similarity between grassland and objects C and D is high, indicating that the spectral camouflage effect of objects C and D is

**Table 1:** Comparison of similarity evaluation methods

| Object | Method | 449–801 nm (1–89) | 449–497 nm (1–13) | 501–597 nm (14–38) | 601–697 nm (39–63) | 701–801 nm (64–89) |
|---|---|---|---|---|---|---|
| Grassland and A | SAM | 0.3807 | 0.0233 | 0.0572 | 0.2204 | 0.1329 |
| | StDev | 0.1309 | 0.1563 | 0.1541 | 0.1381 | 0.0864 |
| | SCC | 0.9657 | 0.9901 | 0.9658 | 0.8817 | 0.8685 |
| | JD-SSI | 0.6539 | 0.7502 | 0.8186 | 0.7908 | 0.3156 |
| Grassland and B | SAM | 0.2909 | 0.0108 | 0.0246 | 0.0311 | 0.2060 |
| | StDev | 0.1354 | 0.0274 | 0.0106 | 0.0133 | 0.2528 |
| | SCC | 0.5939 | 0.9981 | 0.9935 | 0.9873 | 0.3573 |
| | JD-SSI | 0.2749 | 0.1953 | 0.0835 | 0.1025 | 0.6644 |
| Grassland and C | SAM | 0.1054 | 0.0408 | 0.0946 | 0.1718 | 0.0411 |
| | StDev | 0.0611 | 0.0636 | 0.0755 | 0.0572 | 0.0509 |
| | SCC | 0.9692 | 0.9916 | 0.9634 | 0.7983 | 0.9252 |
| | JD-SSI | 0.3111 | 0.2920 | 0.3912 | 0.2959 | 0.2583 |
| Grassland and D | SAM | 0.3152 | 0.0631 | 0.0698 | 0.4016 | 0.0276 |
| | StDev | 0.1300 | 0.1699 | 0.1557 | 0.1288 | 0.0802 |
| | SCC | 0.9562 | 0.9736 | 0.9467 | 0.8012 | 0.9303 |
| | JD-SSI | 0.6111 | 0.7796 | 0.8375 | 0.6925 | 0.2310 |

better. From the perspective of different algorithms in 449–801 nm: Object C has the best camouflage effect while object A has the worst under the SAM algorithm. Object C has the best camouflage effect while object B has the worst under the StDev algorithm. Object C has the best camouflage effect while object B has the worst under the SCC algorithm. Object B has the best camouflage effect while object A has the worst under the JD-SSI algorithm. When evaluating the similarity between grassland and three objects A, C, and D in different bands, the four similarity evaluation methods used reached inconsistent conclusions. This is because these similarity evaluation indicators evaluated the spectral separability of the two objects from different perspectives, and the ground object targets in different bands are likely to exhibit this characteristic. In comparison, the four evaluation indicators unanimously determine that the spectral separability between grassland and object B is strong at 701–801 nm, indicating that 701–801 nm is one of the most effective bands for distinguishing grassland and object B.

## 4 Conclusion and discussion

Spectral uncertainty is one of the key difficulties faced by hyperspectral image processing. Many researchers are committed to reducing the impact of spectral uncertainty on hyperspectral image classification and object detection. Land-based hyperspectral images have many distinct characteristics compared to hyperspectral remote sensing images, especially in terms of spectral uncertainty. There are many methods to reduce the impact of spectral uncertainty, such as early spectral correction, later spectral dimensionality reduction, model optimization, *etc.* This study takes grassland and its camouflages as examples and proposes a method based on Jaccard Distance to measure the spectral separability between objects. Experiments have shown that this method can study spectral similarity from the perspective of distance between sample classes, providing a new approach for spectral band extraction. However, there may be several areas for improvement throughout the entire process from the proposal to application of this method: (1) The number and representativeness of target spectral samples need to be improved, and how to select more typical target spectra during the sampling process is the key to data preparation. In the future, unmanned aerial vehicle hyperspectral real-time imaging equipment can be used to measure more hyperspectral images under different imaging conditions, making the proposed method more convincing. (2) More comprehensive consideration of the intra-class dispersion index and inter-class separability index of the target class. Through the above experiments, it can be found that the situation where the intra-class dispersion index of a single target is smaller and the inter-class separability index between different targets is larger is more conducive to distinguishing two objects. Therefore, in order to find effective bands to distinguish between two types of objects, it is necessary to comprehensively consider these two indicators and weigh them. (3) The purpose of band extraction is to select the bands with the most separability between targets while reducing spectral dimensionality. A simple similarity evaluation method has significant limitations. Therefore, establishing a method that comprehensively considers various separability evaluation indicators is of great significance.

**Funding information:** The authors state no funding involved.

**Author contributions:** All authors have accepted responsibility for the entire content of this manuscript and approved its submission.

**Conflict of interest:** The authors state no conflict of interest.

## References

[1] Khan MJ, Khan HS, Yousaf A, Khurshid K, Abbas A. Modern trends in hyperspectral image analysis: a review. IEEE Access. 2018;6:14118–29.
[2] Xu Z, Liu Y, Gan L, Hu X, Sun Y, Liu M, et al. csBoundary: City-scale road-boundary detection in aerial images for high-definition maps. IEEE Robot Autom Lett. 2022;7:5063–70.
[3] Tong Z, Li Y, Zhang J, He L, Gong Y. MSFANet: Multiscale fusion attention network for road segmentation of multispectral remote sensing data. Remote Sens. 2023;15:1978.
[4] Akgun T, Altunbasak Y, Mersereau RM. Super-resolution reconstruction of hyperspectral images. IEEE Trans Image Process. 2005;14(11):1860–75.
[5] Fauvel M, Tarabalka Y, Benediktsson JA, Chanussot J, Tilton JC. Advances in spectral-spatial classification of hyperspectral images. Proc IEEE. 2013;101(3):652–75.
[6] Bioucas-Dias JM, Plaza A, Camps-Valls G, Scheunders P, Nasrabadi NM, Chanussot J. Hyperspectral remote sensing data analysis and future challenges. IEEE Geosci Remote Sens Mag. 2013;1(2):6–36.
[7] Kruse FA, Perry SL, Caballero A. District-level mineral survey using airborne hyperspectral data, Los Menucos, Argentina. Ann Geophys. 2006;49:83–92.
[8] Ang LM, Seng JKP. Big data and machine learning with hyperspectral information in agriculture. IEEE Access. 2021;9:36699–718.
[9] Honkavaara E, Saari H, Kaivosoja J, Pölönen I, Pesonen L. Processing and assessment of spectrometric, stereoscopic imagery collected using a lightweight UAV spectral camera for precision agriculture. Remote Sens. 2013;5(10):5006–39.
[10] Delegido J, Verrelst J, Meza CM, Rivera JP, Alonso L, Moreno J. A red-edge spectral index for remote sensing estimation of green LAI over agroecosystems. Eur J Agron. 2013;46:42–52.

[11] Mahlein AK, Rumpf T, Welke P, Dehne HW, Plümer L, Steiner U, et al. Development of spectral indices for detecting and identifying plant diseases. Remote Sens Environ. 2013;128:21–30.
[12] Curcio AC, Barbero L, Peralta G. UAV-hyperspectral imaging to estimate species distribution in salt marshes: a case study in the Cadiz Bay (SW Spain). Remote Sens. 2023;15:1419.
[13] Kumar V, Ghosh JK. Camouflage detection using MWIR hyperspectral images. J Indian Soc Remote Sens. 2017;45:139–45.
[14] Qiao Y, Zheng G, Du Z, Ma X, Li J, Moskal LM. Tree-species classification and individual-tree-biomass model construction based on hyperspectral and LiDAR data. Remote Sens. 2023;15:1341.
[15] Nagendra H, Lucas R, Honrado JP, Jongman RHG, Tarantino C, Adamo M, et al. Remote sensing for conservation monitoring: Assessing protected areas, habitat extent, habitat condition, species diversity, and threats. Ecol Indic. 2013;33(oct):45–59.
[16] Barbin DF, Elmasry G, Sun DW, Allen P. Non-destructive determination of chemical composition in intact and minced pork using near-infrared hyperspectral imaging. Food Chem. 2013;138(2–3):1162–71.
[17] Zhao X, Wu B, Xue J, Shi Y, Zhao M, Geng X, et al. Mapping forage biomass and quality of the inner mongolia grasslands by combining field measurements and sentinel-2 observations. Remote Sens. 2023;15:1973.
[18] Lin L, Wang Y, Teng J, Xi X. Hyperspectral analysis of soil total nitrogen in subsided land using the local correlation maximization-complementary superiority (LCMCS) method. Sensors. 2015;15:17990–8011.
[19] Hengbiao Z, Tao C, Dong L, Xia Y, Yongchao T, Weixing C, et al. Combining unmanned aerial vehicle (UAV)-based multispectral imagery and ground-based hyperspectral data for plant nitrogen concentration estimation in rice. Front Plant Sci. 2018;9:936.
[20] Wang R, Liu ZG, Feng HK, Yang PQ, Wang QS, Ni ZY. Extraction and analysis of solar-induced chlorophyll fluorescence of wheat with ground-based hyperspectral imaging system. Spectrosc Spectr Anal. 2013;33(9):2451.
[21] Lunga D, Prasad S, Crawford M, Ersoy O. Manifold-learning-based feature extraction for classification of hyperspectral data: A review of advances in manifold learning. IEEE Signal Proc Mag. 2014;1:31.
[22] Dobigeon N, Tourneret JY, Richard C, Bermudez JCM, McLaughlin S, Hero AO. Nonlinear unmixing of hyperspectral images. IEEE Signal Proc Mag. 2013;31(1):82–94.
[23] Zhu W, You D, Wen J, Tang Y, Gong B, Han Y. Evaluation of linear kernel-driven BRDF models over snow-free rugged terrain. Remote Sens. 2023;15:786.
[24] Cui L, Sun M, Jiao Z, Park J, Agca M, Zhang H, et al. Effectiveness of the reconstructed MODIS typical-angle reflectances on forest biomass estimation. Remote Sens. 2022;14:5475.
[25] Xu J, Zhou X, Han C, Dong B, Li H. SAM-GAN: Supervised learning-based aerial image-to-map translation via generative adversarial networks. ISPRS Int J Geo-Inf. 2023;12:159.
[26] Wang K, Yong B. Application of the frequency spectrum to spectral similarity measures. Remote Sens. 2016;8:344.
[27] Pathak P, Chalopin C, Zick L, Köhler H, Pfahl A, Rayes N, et al. Spectral similarity measures for in vivo human tissue discrimination based on hyperspectral imaging. Diagnostics. 2023;13:195.
[28] Deepthi Devassy BM, George S, Nussbaum P, Thomas T. Classification of forensic hyperspectral paper data using hybrid spectral similarity algorithms. J Chemom. 2022;36:3387.
[29] Chen YS, Zhao X, Jia XP. Spectral-spatial classification of hyperspectral data based on deep belief network. IEEE J Sel Top Appl Earth Obs Remote Sens. 2015;8(6):2381–92.
[30] Jia S, Tang GH, Zhu JS, Li QQ. A novel ranking-based clustering approach for hyperspectral band selection. IEEE Trans Geosci Remote Sens. 2016;54(1):88–102.
[31] Rozinek O, Mareš J. The duality of similarity and metric spaces. Appl Sci. 2021;11:1910.
[32] Kwon N, Lee J, Park M, Yoon I, Ahn Y. Performance evaluation of distance measurement methods for construction noise prediction using case-based reasoning. Sustainability. 2019;11:871.
[33] Kowalczyk P, Izydorczyk J, Szelest M. Evaluation methodology for object detection and tracking in bounding box based perception modules. Electronics. 2022;11:1182.
[34] Jang KE, Kim G, Shin MH, Cho JG, Jeong JH, Lee SK, et al. Field application of a Vis/NIR hyperspectral imaging system for non-destructive evaluation of physicochemical properties in 'Madoka' peaches. Plants. 2022;11:2327.
[35] Zhao J, Zhou B, Wang G, Ying J, Liu J, Chen Q. Spectral camouflage characteristics and recognition ability of targets based on visible/near-infrared hyperspectral images. Photonics. 2022;9:957.